Incorporation of Bone Beam Hardening Correction into Statistical Iterative CT Reconstruction

Bernhard Brendel[a], Thomas Koehler[a], Yoad Yagil[b], and Richard Thomson[c]

Abstract— **A number of different methods for post reconstruction bone beam hardening (BBH) correction are available for conventional FBP reconstruction and are used in commercially available products. An incorporation of these existing methods into statistical iterative reconstruction for CT would be desirable. There are two ways imaginable to incorporate the BBH correction into iterative reconstruction: The first option is to use the beam hardening corrected projections as input for the statistical iterative reconstruction. For this it has to be considered that the noise level in the projection data changes due to the correction. The second option is to incorporate the inverse of the beam hardening correction into the forward projection of the cost function, and derive an update equation from this modified cost function. Both methods are implemented and compared based on simulated data with respect to artifact suppression, image noise, and speed of convergence.**

I. Introduction

In recent years, the attention to iterative reconstruction methods for CT has grown considerably, since the increasing power of todays computation hardware decreased reconstruction times to a tolerable level. Iterative reconstruction methods have the advantage as compared to conventional filtered back projection (FBP) that image quality can be increased significantly. The incorporation of a statistical model for the noise in the acquired data, the application of a detailed geometrical model, and the consideration of a priori knowledge about the image decrease noise and increase resolution in the image [1].

To further improve image quality, also other important physical effects (apart from noise) influencing the data acquisition should be modeled in the iterative reconstruction process. In conventional FBP reconstruction, a number of these effects are already considered in pre- and postprocessing steps. One of these effects is beam hardening, which may lead to artifacts if it is not handled properly during reconstruction [2]. In FBP based methods, it is corrected in two steps: The beam hardening due to soft tissue is corrected in a preprocessing step, while the beam hardening due to bone is accounted for in a postprocessing step, which itself includes normally at least one forward projection step and one reconstruction step [3, 4].

Due to the sometimes severe artifacts introduced by beam hardening, it is necessary to consider it also in iterative reconstruction. A number of methods have been introduced to avoid beam hardening artifacts in iterative reconstruction [5, 6]. Most of them defer significantly from the methods used in the pre- and postprocessing of conventional FBP reconstruction, and extensively use knowledge about the spectral properties of tube, detector, and scanned object. Thus, an application of these methods may results in additional effort regarding implementation, spectral characterization of the CT system, and testing.

To avoid this, we discuss in the following two ways to incorporate a beam hardening correction scheme originally designed for FBP based reconstruction, into iterative reconstruction. The first way is to use the beam hardening corrected projection data as input for the iterative reconstruction. For this scenario, it has to be considered that the noise level of the projection data changes during the correction, and the noise assumptions for the iterative reconstruction have to be adapted accordingly. This can be done by propagating the noise through the correction steps. The second way is to incorporate the inverse of the correction steps in the forward projection of the cost function for the iterative reconstruction, and derive an update equation from this modified cost function. Both ways are explained in the following section in detail, along with the applied beam hardening correction scheme.

II. Method

Conventional FBP reconstruction is based on the assumption that the input data represents line integrals of the X-ray attenuation μ of an object:

$$l_i = \int_{L_i} \mu\left(\mathbf{x}\right) \mathrm{d}l \tag{1}$$

Here, l_i denotes the line integral of the ith measurement along ray L_i. A calculation of these line integrals is easy, if the X-ray radiation used for data acquisition is monochromatic. According to Beer's law, the measured intensities I_i at the detector are then

$$I_i = I_0 \cdot \mathrm{e}^{-\int_{L_i} \mu(\mathbf{x})\mathrm{d}l}, \tag{2}$$

with I_0 being the intensity of the X-ray radiation before the object. The line integrals can then simply be determined by

$$l_i = \log \frac{I_0}{I_i}. \tag{3}$$

In reality however, the applied X-ray radiation covers a broad spectrum of energies, and the X-ray attenuation depends on the energy E of the photons. Thus, the measured intensities are modeled as follows:

$$I_i = I_0 \cdot \int S\left(E\right) \mathrm{e}^{-\int_{L_i} \mu(\mathbf{x},E)\mathrm{d}l} \mathrm{d}E \tag{4}$$

Here, $S(E)$ is the probability, that a detected photon has the energy E.

[a] Philips Technologie GmbH, Innovative Technologies, Research Laboratories, Hamburg, Germany
[b] Philips Healthcare, Haifa, Israel
[c] Philips Healthcare, Cleveland, OH

For a first step, we assume, that the object consists of only one material (e.g., water), with attenuation spectrum $\mu_{\mathrm{w}}(E)$. Furthermore, it is assumed that the material distribution is spatially varying and modeled by $\rho_{\mathrm{w}}(\mathbf{x})$, which stands here for the volume fraction containing water at location $\mathbf{x}$. The energy dependent attenuation in each location is then given by $\mu(\mathbf{x}, E) = \mu_{\mathrm{w}}(E)\rho_{\mathrm{w}}(\mathbf{x})$, and Eq. (4) can be written as

$$I_i = I_0 \cdot \int S(E)\, \mathrm{e}^{-T_{\mathrm{w}i}\mu_{\mathrm{w}}(E)} \mathrm{d}E, \tag{5}$$

with $T_{\mathrm{w}i} = \int_{L_i} \rho_{\mathrm{w}}(\mathbf{x})\mathrm{d}\mathbf{x}$ being the path length of water along the ray. The line integral we are looking for is $l_i = \mu_{\mathrm{w}}(\overline{E}) \cdot T_{\mathrm{w}i}$, with $\overline{E}$ being a "mean energy", derived from $S(E)$ [3]. As one can see, the relationship between l_i and $\log(I_0/I_i)$ is not trivial, and depends on the spectra $S(E)$ and $\mu_{\mathrm{w}}(E)$. Nevertheless, $\log(I_0/I_i)$ is a monotonic and only weakly nonlinear function in $T_{\mathrm{w}i}$. Thus, the mapping of $\log(I_0/I_i)$ onto l_i can be approximated by a low order polynomial. This is conventionally done in the water beam hardening (WBH) correction step [3]. The coefficients of the polynomial can be calculated from Eq. (5) or derived from a calibration measurement.

This correction step eliminates beam hardening artifacts due to water and soft tissue, but if the object contains additionally bone, artifacts remain due to the fact that the attenuation spectrum of bone $\mu_{\mathrm{b}}(E)$ differs significantly from water. To solve this problem, we have to consider Eq. (4) for two materials:

$$I_i = I_0 \cdot \int S(E)\, \mathrm{e}^{-T_{\mathrm{w}i}\mu_{\mathrm{w}}(E) - T_{\mathrm{b}i}\mu_{\mathrm{b}}(E)} \mathrm{d}E. \tag{6}$$

Now, the line integral we are looking for is $l_i = \mu_{\mathrm{w}}(\overline{E}) \cdot T_{\mathrm{w}i} + \mu_{\mathrm{b}}(\overline{E}) \cdot T_{\mathrm{b}i}$, but a mapping of $\log(I_0/I_i)$ onto l_i is no longer possible. For a certain value of I_i, different combinations of $T_{\mathrm{w}i}$ and $T_{\mathrm{b}i}$ fulfill Eq. (6), but they lead to different values for l_i. Thus, one common way to correct the beam hardening for two materials is to estimate in a preliminary image (e.g., reconstructed with WBH corrected projection data) for each pixel $\rho_{\mathrm{w}}(\mathbf{x})$ and $\rho_{\mathrm{b}}(\mathbf{x})$ based on the reconstructed attenuation value [4]. $\rho_{\mathrm{w}}(\mathbf{x})$ and $\rho_{\mathrm{b}}(\mathbf{x})$ can then be forward projected to get an estimate of $T_{\mathrm{w}i}$ and $T_{\mathrm{b}i}$. One of both or both are then utilized in combination with Eq. (6) to estimate l_i.

There are different methods described to estimate l_i in a two material scenario [3, 4, 7]. We use here one, which has similarities with [7]. It is based on the idea, that we can do a correction similar to the WBH correction for any given attenuation spectrum. For example, a measurement with a certain fraction of attenuation by water with respect to the complete attenuation $R = T_{\mathrm{w}i} \cdot \mu_{\mathrm{w}}(\overline{E}) / (T_{\mathrm{b}i} \cdot \mu_{\mathrm{b}}(\overline{E}) + T_{\mathrm{w}i} \cdot \mu_{\mathrm{w}}(\overline{E}))$ has the effective normalized attenuation spectrum $m_R(E) = R \cdot \mu_{\mathrm{w}}(E)/\mu_{\mathrm{w}}(\overline{E}) + (1-R) \cdot \mu_{\mathrm{b}}(E)/\mu_{\mathrm{b}}(\overline{E})$. With this, Eq. (6) becomes

$$I_i = I_0 \cdot \int S(E)\, \mathrm{e}^{-l_i m_R(E)} \mathrm{d}E. \tag{7}$$

Since $m_R(E)$ is constant for a given R, $\log(I_0/I_i)$ can unambiguously be mapped onto l_i using Eq. (7) if R is known.

Thus, if for a number of fraction values R polynomials $f_R(\log(I_0/I))$ are estimated based on Eq. (7) or on calibration measurements, these can be applied to correct the projection data.

$$l_i = f_{R_i}\left(\log \frac{I_0}{I_i}\right) = \sum_{n=0}^{N} \alpha_{R_i,n} \cdot \log^n \frac{I_0}{I_i} \tag{8}$$

Here, R_i is the fraction value for measurements i, which is estimated based on preliminary reconstructions as explained above. The correction can be applied iteratively, i.e., the reconstruction based on the corrected data can be used to refine the values R_i for an improved correction of the data and so on.

The next step is to combine the correction of Eq. (8) with an iterative reconstruction scheme. We use a log-likelihood approach assuming Gaussian noise on the line integral data, resulting in the cost function [1]

$$C = \|\mathbf{D}(\mathbf{A}\mu - \mathbf{l})\|^2 = \sum_{i=1}^{M} d_{ii}^2 \cdot \left(\sum_{j=1}^{J} a_{ij}\mu_j - l_i\right)^2. \tag{9}$$

μ is a vector with entries μ_j containing a discretized version of the image to reconstruct, $\mathbf{A}$ is the forward projection matrix, $\mathbf{l}$ is the vector with the line integral data l_i, and $\mathbf{D}$ is a diagonal weighting matrix with the inverse standard deviations of the line integral data l_i as entries d_{ii}. Sums are running over all J image pixels and over all M measurements.

For the monochromatic case, the entries l_i of $\mathbf{l}$ are simply $\log(I_0/I_i)$. Based on the assumption that the standard deviations of the measured intensities are $\sigma_{I_i} = \sqrt{I_i}$, and according to error propagation the standard deviations of the line integrals are $\sigma_{l_i} = 1/\sqrt{I_i}$, and thus the diagonal Matrix $\mathbf{D}$ has entries $d_{ii} = 1/\sigma_{l_i} = \sqrt{I_i}$ (see also [1]).

There are now two options to incorporate the beam hardening correction as given in Eq. (8) in the cost function (9). First, we can use the corrected projection data l_i instead of $\log(I_0/I_i)$ in vector $\mathbf{l}$. For this case, Eq. (9) is still valid, but we have to choose the entries of $\mathbf{D}$ properly. Neglecting the influence of the projection noise on the estimation of the values R_i (and thus on the choice of the coefficients for the correction polynomial), we can determine them as $d_{ii} = \sqrt{I_i} / \sum_n \alpha_{R_i,n} \cdot n \cdot \log^{n-1}(I_0/I_i)$.

Second, we can estimate polynomials $f_{R_i}^{-1}$ solving the inverse problem of mapping l_i onto $\log(I_0/I_i)$, and apply these inverse polynomials to the forward projected values $\mathbf{A}\mu$. The cost function is then given by

$$C = \sum_i I_i \cdot \left(f_{R_i}^{-1}\left(\sum_j a_{ij}\mu_j\right) - \log \frac{I_0}{I_i}\right)^2. \tag{10}$$

For both cost functions we derived SPS-like update equations according to [8]. Since Eq. (9) is quadratic and Eq. (10) is almost quadratic (with the valid assumption that $f_{R_i}^{-1}$ is only weakly nonlinear), we calculate the update as Newton-Raphson steps of a separable surrogate function of the respective cost function. To keep equations short,

we abbreviate $h_i = \log(I_0/I_i)$ in the following. The update equation for cost function (9) can be written as

$$\mu_j^{(k+1)} = \mu_j^{(k)} - \frac{\sum_i a_{ij} \cdot d_{ii}^2 \cdot \left(\sum_{j'} a_{ij'} \mu_{j'}^{(k)} - f_{R_i}(h_i)\right)}{\sum_i a_{ij} \cdot d_{ii}^2 \cdot \sum_{j'} a_{ij'}} \tag{11}$$

with $d_{ii} = \sqrt{I_i} / \sum_n \alpha_{R_i,n} \cdot n \cdot h_i^{n-1}$ (see above). $\mu_j^{(k)}$ are the image values in the kth iteration step. For the cost function (10) the update equation is given by

$$\mu_j^{(k+1)} = \mu_j^{(k)} - \frac{\sum_i a_{ij} \cdot I_i \cdot \left(f_{R_i}^{-1}\left(\sum_{j'} a_{ij'} \mu_{j'}^{(k)}\right) - h_i\right) \cdot \dot{f}_{R_i}^{-1}(h_i)}{\sum_i a_{ij} \cdot I_i \cdot \sum_{j'} a_{ij'} \cdot \left(\dot{f}_{R_i}^{-1}(h_i)^2 + f_{R_i}^{-1}(h_i) \ddot{f}_{R_i}^{-1}(h_i)\right)} \tag{12}$$

with $\dot{f}_{R_i}^{-1}(h_i)$ and $\ddot{f}_{R_i}^{-1}(h_i)$ being the first and second derivative of $f_{R_i}^{-1}$ with respect to h_i.

We extended the update equations to include ordered subsets and regularization (see [8] for details). We then implemented both iterative reconstruction methods. The Polynomials f_R and f_R^{-1} are estimated using a least square fit based on Eq. (7) with a polynomial order of 11 for 500 equidistantly spaced values of R.

For the method based on Eq. (11) we do the beam hardening correction before iterative reconstruction, with the "conventional" approach as follows: A FBP reconstruction is performed based on WBH corrected projection data. The reconstructed image is used to calculate $\rho_{\mathrm{w}}(\mathbf{x})$ and $\rho_{\mathrm{b}}(\mathbf{x})$. Based on that the values R_i are estimated and projection data is BBH corrected using Eq. (8). This process is repeated a second time using the BBH corrected projection data as input (but the observed improvement is very low). Then, the values of d_{ii} are calculated. The corrected projection data of the second step as well as the values d_{ii} are the input for the iterative reconstruction method, i.e., the values of R_i are not updated during the reconstruction. This method is named "BBH external" in the following.

For the method based on Eq. (12) uncorrected projection data is used as input. The values R_i are calculated during reconstruction. This leads to one additional forward projection per update to determine $T_{\mathrm{b}i}$ from $\rho_{\mathrm{b}}(\mathbf{x})$, increasing computation time substantially. The method is called "BBH internal" in the following.

Both methods are evaluated based on simulated 2D spectral data of the FORBILD head phantom. We simulated an axial CT scan of a single-row detector with 672 elements, a source-detector distance of 1040 mm, source iso–center distance of 570 mm, fan–angle of 52.138°, and 2320 views over 360°. The tube spectrum is a 120kV tungsten spectrum, filtered by 0.6 mm Titanium and 0.8 mm Aluminum. The detector is assumed to be ideal energy integrating. The absorption spectra of soft tissue and bone are taken from [9, 10].

III. Results

We analyze the reconstructions of the simulated data with respect to artifacts, noise, and speed of convergence.

For the analysis of the artifacts, we use noise free simulated data. Nevertheless, the noise model described above is used for iterative reconstruction. In Fig. 1 the FBP reconstructions of the WBH corrected data and of the BBH corrected data are given. One can clearly see that the BBH correction suppresses the BBH artifacts, however there are some weak remaining artifacts (marked by arrows).

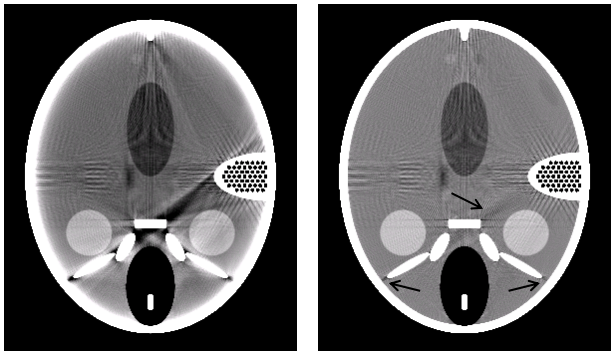

Fig. 1. FBP reconstructions. Left: WBH corrected projection data. Right: BBH corrected projection data. (Window/Level: 50/100 HU)

Iterative reconstructions are performed with 116 equally distributed projection subsets. For the noise free case, a weak Huber regularization is applied to suppress aliasing artifacts ($\delta = 1$ HU). For both methods the BBH corrected FBP image is used as start image. In Fig. 2, reconstruction results after 100 iterations are shown. While, as expected, the BBH external reconstruction has weak remaining artifacts similar to the BBH corrected FBP reconstruction (Fig. 1, right), the BBH internal reconstruction suppresses bone artifacts even better. This is due to the repeated refinement of the R_i values during reconstruction. However,

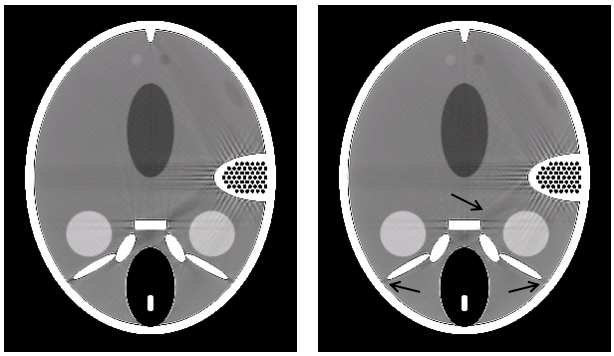

Fig. 2. Iterative reconstructions using a BBH corrected start image. Left: BBH external method. Right: BBH internal method. Window/Level: 50/100 HU

the improvement of the artifact suppression is a rather slow converging process, as can be seen in Fig. 3. Here the reconstructed attenuation value of one image pixel within one of the artifact regions is shown over the first 200 iterations. It takes roughly 100 iterations (corresponding to 11,600 updates of the R_i values) until the final improved artifact level is reached. The intermediate results degrade if a WBH corrected FBP image is used as start image.

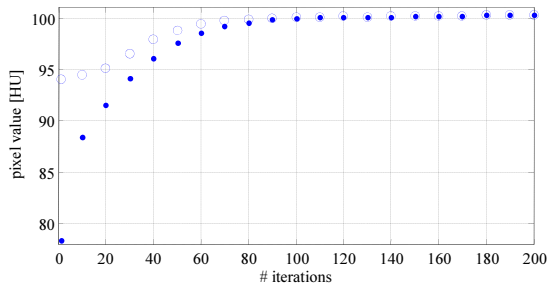

Fig. 3. Value of one image pixel in the artifact region denoted by the bottom right arrow in Fig. 2 over the number of iterations for the BBH internal method. Circles: BBH corrected FBP image as start image. Dots: WBH corrected FBP image as start image.

To analyze the noise in the reconstructed images, Poisson noise was added to the simulated intensity data. For the reconstructions the regularization strength was a bit increased to avoid salt-and-pepper noise in the images. Reconstruction results are shown in Fig. 4 for 100 iterations. In the difference image it becomes obvious, that the main differences between the two images are due to the different artifact suppression level, while differences in the noise pattern are very weak, even in the representation with a 5 HU window. This is verified by SNR measurements in homogeneous regions, which show a roughly 5 % better SNR for the BBH external method. The differences in the bone regions are due to differences in the BBH suppression, but it has to be kept in mind, that the window of 5 HU is extremely low as compared to the absolute attenuation values of bone.

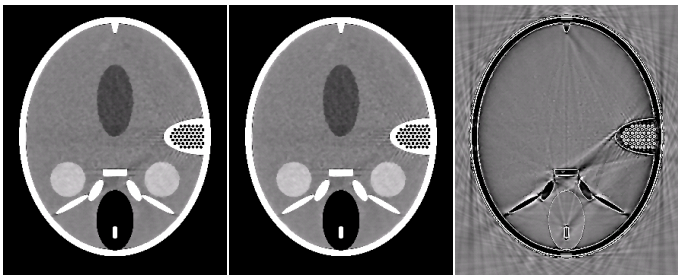

Fig. 4. Iterative reconstructions from noisy projection data. Left: BBH external method. Middle: BBH internal method. (Window/Level: 50/100 HU) Right: Difference image. (Window: 5 HU)

To analyze the convergence, we compared the differences between the reconstructions of the two methods after 100 iterations (when the improvement of the bone artifact suppression for the BBH internal is nearly finished) and after 1000 iterations:

$$\Delta = \mu^{1000}_{\text{internal}} - \mu^{1000}_{\text{external}} - (\mu^{100}_{\text{internal}} - \mu^{100}_{\text{external}}) \qquad (13)$$

Here $\mu^{n}_{\text{internal}}$ denotes the reconstruction of the BBH internal method after n iterations ("external" analogous). This has the advantage that the progress over 900 iterations can be compared, while the differences between the reconstruction methods due to the different BBH suppression is widely eliminated. The Δ-image is visualized in Fig. 5. Apart from the outer rim of the skull, the differences are below a few HU, indicating that the convergence of both methods is very similar. The larger differences at the outer rim of the skull can be explained by the different bone artifact suppression, resulting especially in different attenuation values at the outer rim of the skull (see also Fig. 4). The different contrast between air and skull leads to different amplitudes of overshoots for the two methods, and in consequence to the differences observed here.

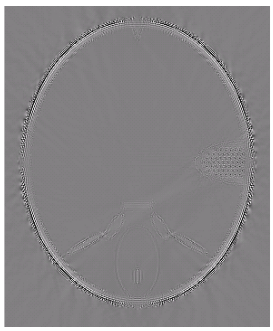

Fig. 5. The Δ-image as defined by Eq. (13). (Window: 20 HU)

IV. Discussion

We introduced and compared two methods to incorporate a BBH correction method, which is originally designed for FBP based reconstruction methods, in an iterative reconstruction scheme. Both perform very similar with respect to noise and speed of convergence. The BBH internal method has the advantage that it suppresses BBH artifacts slightly better, but the reduction of the BBH artifacts converges quite slowly. This slow convergence explains also the observed vanishing effect of the second application of the BBH correction for conventional FBP based methods. The advantage of the BBH external method on the other hand is the clearly reduced computational effort due to the avoidance of an additional forward projection per update step.

The idea introduced here is not only applicable to BBH correction, but also to the correction of other physical effects incorporated in pre- or postprocessing steps of conventional FBP methods.

References

[1] Jean-Baptiste Thibault, Ken D Sauer, Charles A Bouman, and Jiang Hsieh, *Med. Phys.*, vol. 34, no. 11, pp. 4526–4544, 2007.
[2] J. Hsieh, *Computed Tomography - Principles, Design, Artifacts, and Recent Advances*, SPIE, Bellingham, Washington, 2003.
[3] G. T. Herman, *IEEE Trans. Med. Imag.*, vol. MI-2, no. 3, pp. 128–135, 1983.
[4] P. K. Kijewski and B. E. Bjärngard, *Med. Phys.*, vol. 5, no. 3, pp. 209–214, 1978.
[5] B. De Man, J. Nuyts, P. Dupont, G. Marchal, and P. Suetens, *IEEE Trans. Med. Imag.*, vol. 20, no. 10, pp. 999–1008, 2001.
[6] M. Abella and J.A. Fessler, in *IEEE International Symposium on Biomedical Imaging*, 2009, pp. 165–168.
[7] X. Mou, S. Tang, T. Luo, Y. Zhang, and H. Yu, in *Medical Imaging 2008*, 2008.
[8] J. A. Fessler, "Statistical image reconstruction methods for transmission tomography," in *Handbook of Medical Imaging, Vol. 2*, M. Sonka and J. M. Fitzpatrick, Eds., chapter 1, pp. 1–70. SPIE Press, Bellingham, WA, 2000.
[9] *ICRU Report 44*, 1989.
[10] *ICRU Report 46*, 1992.